Science of the Total Environment 667 (2019) 112–123

Contents lists available at ScienceDirect

Science of the Total Environment

journal homepage: www.elsevier.com/locate/scitotenv

# Human-induced eutrophication dominates the bio-optical compositions of suspended particles in shallow lakes: Implications for remote sensing

Dong Liu [a], Hongtao Duan [a,*], Shujie Yu [b], Ming Shen [a], Kun Xue [a]

[a] Key Laboratory of Watershed Geographic Sciences, Nanjing Institute of Geography and Limnology, Chinese Academy of Sciences, Nanjing 210008, China
[b] Ocean College, Zhejiang University, Zhoushan 316021, China

## HIGHLIGHTS

- Lakes along the middle and lower reaches of Yangtze River were seriously eutrophic.
- Suspended particle compositions were dominated by human-induced eutrophication.
- Bio-optical compositions of suspended particles differed by trophic state index.
- Monitoring suspended particle compositions using satellite data was achievable.

## GRAPHICAL ABSTRACT

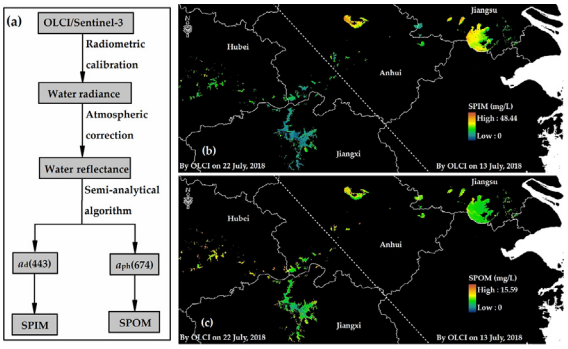


## ARTICLE INFO

*Article history:*
Received 17 December 2018
Received in revised form 7 February 2019
Accepted 24 February 2019
Available online 25 February 2019

Editor: Damia Barcelo

*Keywords:*
Bio-optical composition
Suspended particulate matter
Trophic state index
Remote sensing
Yangtze River

## ABSTRACT

Suspended particulate matter (SPM) is generally divided into inorganic (SPIM) and organic (SPOM) parts; they come from different sources, and have different impacts on the optical properties and/or water quality of lake. However, in a specific remote sensing process, they are not retrieved separately. Using *in-situ* data of 59 lakes along the middle and lower reaches of the Yangtze River (MLR-YR) in dry season (April) and wet season (August) in 2012, we first studied the absorption properties and sources of different SPM. On this basis, we proposed a workflow for simultaneously estimating SPIM and SPOM from satellite data. Our results are as follows: Bio-optical compositions of SPM in these eutrophic shallow lakes tempo-spatially varied greatly and were dominated by human-induced eutrophication. Phytoplankton contributed 18.42 ± 18.92% of SPIM and 26.22 ± 19.24% of SPOM in April 2012, but 30.4 ± 23.41% of SPIM and 47.03 ± 18.1% of SPOM in August 2012. The trophic state index explained 42.84% of SPOM variation in April 2012, and 54.64% in August 2012. Moreover, there were strong linear relationships between SPIM concentration and non-algal particle absorption coefficient (Pearson's $r = 0.73$; $p < 0.01$) and between SPOM concentration and phytoplankton absorption coefficient ($r = 0.76$; $p < 0.01$). Based on these results, SPIM and SPOM concentrations in the lakes along the MLR-YR could be retrieved from OLCI/Sentinel-3A satellite data, respectively. This study has a great significance for real-time monitoring and managing aquatic environment in various eutrophic and/or shallow lakes as a group.


## 1. Introduction

Suspended particulate matter (SPM) is a major factor in reducing water transparency, changing underwater light field, and affecting

* Corresponding author.
*E-mail address:* htduan@niglas.ac.cn (H. Duan).

https://doi.org/10.1016/j.scitotenv.2019.02.366
0048-9697/

primary productivity (Cao et al., 2017; Gernez et al., 2014). SPM also affects the distributions of aquatic vegetation and light-dependent aquatic organisms, and has important scientific and practical significance on aquatic ecological environment (Duan et al., 2009b). In lakes, especially the shallow ones that are the most abundant type in the global landscape (Meerhoff and Jeppesen, 2009), wind-induced sediment resuspension plays an important role in controlling SPM concentration (Markensten and Pierson, 2003; Zhang et al., 2006). Meantime, numerous lakes face eutrophication due to human activities (Duan et al., 2014; Jiang, 2010; Lund, 1967). Among the 2058 lakes with areas larger than 25 $km^2$ globally, 63.1% are in eutrophic state (Wang et al., 2018). As a result of eutrophication, phytoplankton production grows sharply and even leads to algal bloom (Duan et al., 2009a; Kong and Gao, 2005; Paerl et al., 2011). SPM includes organic (SPOM) and inorganic (SPIM) parts. SPOM contains the organic fractions of phytoplankton, detritus, and bacteria, *etc.* (Liu, 2017). Resuspended sediment is characterized by high SPIM content and low SPOM content, but on the contrary for phytoplankton. Moreover, biochemical decomposition of SPOM will lead to oxygen depletion, poor water quality, and even fish death (Kong and Gao, 2005; Paerl et al., 2011), but not for SPIM. Therefore, distinguishing the sources and proportions of SPIM and SPOM are of great significance for understanding the changing causes of water transparency and quality.

As a scientific, rapid, and large coverage investigation tool, satellite remote sensing has been widely applied to monitor aquatic environment variables, such as SPM or turbidity (Hou et al., 2017; Shi et al., 2015b; Zhang et al., 2016), phytoplankton (Duan et al., 2017; Gons et al., 2002; Simis et al., 2005), and carbon cycle (Duan et al., 2014; Jiang et al., 2015; Kutser et al., 2015). However, most of these studies focused on only one or several large lakes (Duan et al., 2017; Feng et al., 2012; Jiang et al., 2015; Kutser et al., 2015; Shi et al., 2015b), and only few studies were on group lakes using empirical algorithms (Duan et al., 2014; Hou et al., 2017). Moreover, none of these studies focused on SPIM and/or SPOM individually up to now.

Satellite ocean color sensors, the moderate resolution imaging spectroradiometer (MODIS) and medium resolution imaging spectrometer (MERIS), for examples, were often used to monitor lake environment (Eleveld, 2012; Feng et al., 2012; Shi et al., 2015b). However, these sensors were not designed for monitoring water quality (Toming et al., 2017). The ocean land color instrument onboard the Sentinel-3 satellite series (OLCI/Sentinel-3) opened a new era of water quality monitoring. With special spectral configurations in red and near-infrared bands and high signal-to-noise ratios, OLCI/Sentinel-3A is the first ocean color sensor designed for monitoring water quality of optically complex coastal and inland waters (Toming et al., 2017). OLCI/Sentinel-3A and -3B were launched in October 2016 and April 2018, respectively. Sentinel-3C and -3D are to be launched from 2021 onwards (https://space.skyrocket.de/). OLCI/Sentinel-3 will be one of the main sensors for monitoring inland waters within the next15 years (Shen et al., 2017).

To monitor SPIM and SPOM individually, we need to figure out absorption properties of suspended particles in eutrophic shallow lakes. On the one hand, the absorption properties of various suspended particles are important in determining remote sensing signal, and in distinguishing organic and/or inorganic matters (Bricaud et al., 2010; Xue et al., 2017). On the other hand, absorption properties of suspended particles are often related to water constituent concentrations, for examples, phytoplankton and non-algal particle (NAP) (Shi et al., 2013; Xue et al., 2017; Ylöstalo et al., 2014). Knowing absorption variation with environmental factors is a prerequisite for parameterizing bio-optical models, such as the quasi-analytical algorithm (QAA) (Lee et al., 1998, 2002), and developing robust remote sensing algorithms.

The middle and lower reaches of the Yangtze River (MLR-YR) is one representative region with dense freshwater lakes in China (Ma et al., 2010; Zhang et al., 2019), serving critical roles in supporting water resources (Hou et al., 2017). The MLR-YR region contains 18.57% of lakes in mainland China, among which 529 are larger than 1 $km^2$ (Ma et al., 2010). Most lakes along the MLR-YR are characterized as eutrophic and shallow (Duan et al., 2014; Shi et al., 2013). To monitor suspended particulate compositions in the lakes along the MLR-YR, we first paid attention to bio-optical compositions of suspended particles in different lakes and their relations to eutrophication. Then, we studied tempo-spatial variation of bio-optical compositions and impact factors on such compositions. Finally, we proposed a remote sensing flowchart for simultaneously retrieving SPIM and SPOM in eutrophic and shallow lakes along the MLR-YR.

## 2. Materials and methods

### 2.1. Study area

With a total drainage area of $1.8 \times 10^6$ $km^2$ and length of 6300 km, the Yangtze River (also known as "Changjiang River") is the longest river in Asia and third longest in the world (Duan et al., 2014; Liu et al., 2015; Wang et al., 2012). With gentle gradient and wide watercourse, the most downstream river reach with length of ~1800 km is collectively called the MLR-YR (Duan et al., 2014; Hou et al., 2017; Wang et al., 2014; Zhang et al., 2014). Many lakes are located along the mainstream of the Yangtze River (Fig. 1), and most of them are characterized as shallow (Guo and Li, 2003; Qin, 2004; Zhang et al., 2006). Under extensive anthropogenic influences (Duan et al., 2014; Hou et al., 2017; Wang et al., 2014), most lakes are also characterized by eutrophication and even suffered from serious water quality problem, leading to decreasing available water storage, fish productivity, and wetland vegetation coverage, *etc.* (Duan et al., 2014; Hou et al., 2017).

### 2.2. Field data collection

To investigate bio-optical compositions of suspended particles in the lakes along the MLR-YR, two seasonal cruises were conducted in 2012. In April 2012 (dry season), surface waters at 174 stations for 56 lakes (2–4 stations per lake) were collected (Fig. 1). In August 2012 (wet season), surface waters at 158 stations for 54 lakes were collected (Fig. 1). Surface water (to 30 cm water depth at most) was sampled using a *Niskin* sampler (*General Oceanics Inc. USA*). In each fieldwork period, Secchi disk depth (SDD), indicating illuminance level as a function of water depth, was also measured using a 20-cm-diameter disk painted in black/white quarters (Preisendorfer, 1986).

#### 2.2.1. Constituent concentrations

*In-situ* water samples were filtered through pre-combusted (450 °C for 6 h) *Whatman* GF/F filters (0.7-μm pore size and 47-mm diameter) to collect SPM. To remove dissolved organic matter sorbed to particulate matter, the SPM samples were washed with three 2.5–5.0 mL of purified Milli-Q water by following NASA's protocols (Mueller et al., 2003). Total SPM weight was determined gravimetrically with a precision of 0.01 mg by drying and weighing the SPM sample (40 °C for 6 h) more than once (Strickland and Parsons, 1972). SPM samples were then combusted (550 °C for 3 h) to remove SPOM, and weighed again to get SPIM weight (Strickland and Parsons, 1972). By subtracting SPIM weight from SPM weight, we obtained SPOM weight. Finally, we calculated their concentrations by dividing SPM, SPIM, and SPOM weights by the filtration volume.

*In-situ* water samples were filtered through *Satorius* cellulose acetate filters (0.45-μm pore size and 47-mm diameter) to collect chlorophyll *a* (Chl-*a*). The filtrate was also taken as total nitrogen (TN), total phosphorus (TP), and chemical oxygen demand (COD) samples. Using a *Shimadzu* UV2401 Spectrophotometer, Chl-*a* concentration was spectrophotometrically determined by the standard spectrophotometric method (Knap et al., 1994). After persulfate digestion, TN and TP concentrations were measured through spectrophotometric analysis using the *Shimadzu* UV2401 spectrophotometer (APHA, 1995). Chemical oxygen demand

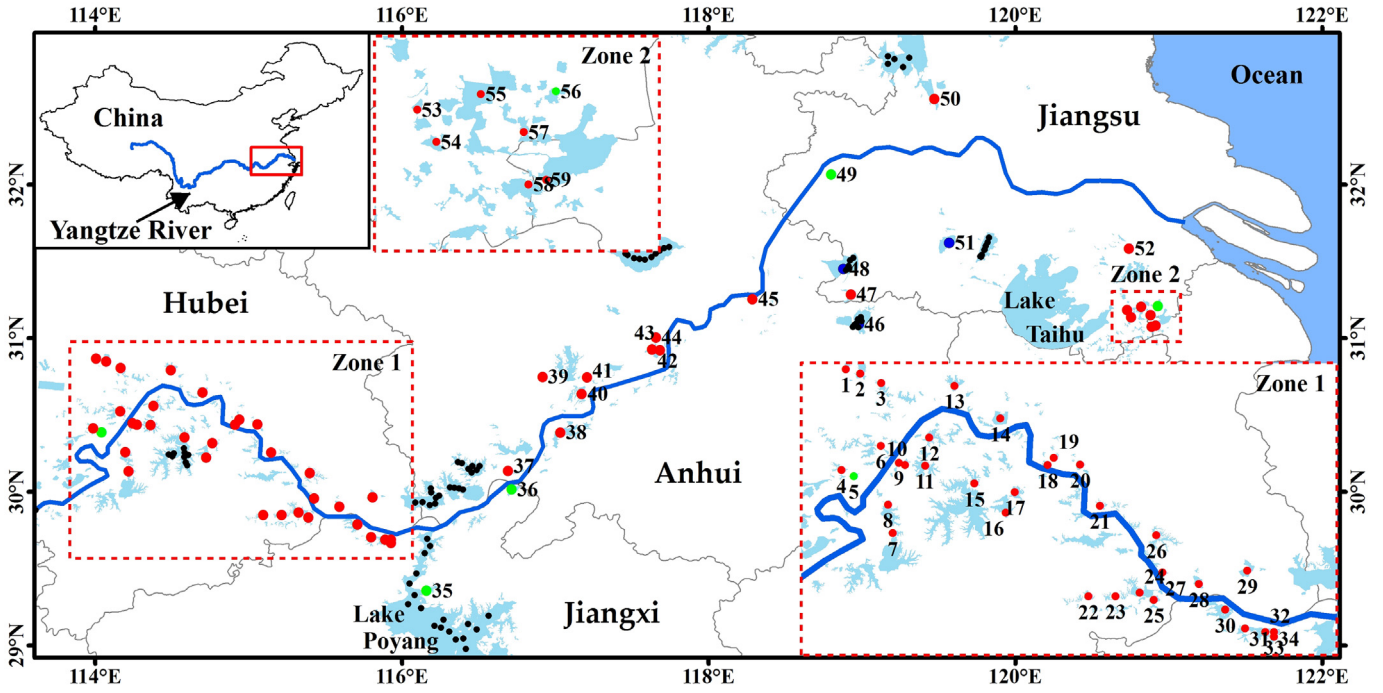


**Fig. 1.** Lakes in the MLR-YR region. The red points (●) denote sampled lakes in both April and August 2012, 51 in all. The green points (●) denote sampled lakes only in April 2012, 5 in all. The blue points (●) denote sampled lakes only in August 2012, 3 in all. The dark points (●) denote sampled stations in July 2018, 80 in all. For more details, please refer to Table S1 in the supplementary material file. The administrative province boundary dataset was sourced from the National Geomatics Center of China (http://ngcc.sbsm.gov.cn/).

(COD) was determined by the potassium permanganate-boiling method (APHA, 1995).

*2.2.2. Absorption coefficients of suspended particulate compositions*

*In-situ* water samples were also filtered through *Whatman* GF/F filters (without pre-combustion) to gather total suspended particle. Using a *Shimadzu* UV2600 spectrophotometer, optical density of total suspended particle ($OD_p$) was determined by the quantitative filter technique (Spinrad and Mitchell, 1990). The total suspended particulate sample was then bleached with sodium hypochlorite to remove phytoplankton pigment to get NAP. Similarly to $OD_p$, optical density of NAP ($OD_d$) was also measured. After measuring $OD_p$ *and* $OD_d$, optical density of a blank *Whatman* GF/F filter wetted with purified Mill-Q water was also measured and taken as the baseline (Ma et al., 2006; Xue et al., 2017).

After lab measurements, background noise was corrected by subtracting corresponding optical density at 750 nm from $OD_p$ and $OD_d$, respectively. Using the method by Cleveland and Weidemann (1993), we further corrected the path-length amplification effect caused by multiple scattering (Ylöstalo et al., 2014). After above corrections, we calculated absorption coefficients of total suspended particle ($a_p$) and NAP ($a_d$) (Cleveland and Weidemann, 1993; Ma et al., 2006; Xue et al., 2017):

$$ai(\lambda) = 2.303 \times ODi(\lambda) \times Af/V \quad (1)$$

where λ represents a specific wavelength from 350 to 750 nm, $A_f$ denotes the effective filtration area, and $V$ denotes the filtration volume. Phytoplankton absorption coefficient ($a_{ph}$) was then calculated by subtracting $a_d$ from $a_p$. The specific absorption coefficients of NAP ($a_d^*(\lambda)$) and phytoplankton ($a_{ph}^*(\lambda)$) were calculated by dividing $a_d$ and $a_{ph}$ by SPIM and Chl-*a* concentrations, respectively (Bricaud et al., 1998, 2010; Ma et al., 2006; Xue et al., 2017; Ylöstalo et al., 2014).

*2.2.3. Validation datasets*

In July 2018, a cruise was also conducted to survey bio-optical properties of suspended particles in the lakes along the MLR-YR (Fig. 1). *In-situ* SPIM, SPOM, $a_d$, and $a_{ph}$ data were collected. All these variables were measured by following the methods described above. In sum, samples at 80 stations were collected (Fig. 1).

When collecting water samples, remote sensing reflectance of water surface ($R_{rs}$) was also measured using an *ASD FieldSpec Spectroradiometer* (*USA*). $R_{rs}$ was only measured from 8:00 a.m. to 4:00 p.m. and under clear sky or stable solar illumination. As a result, $R_{rs}$ was only measured at 58 stations. For details about $R_{rs}$ measurement, please refer to Mueller et al. (2003).

*2.3. Satellite products and processing*

Daily surface vector wind at 10-m height on the sampling day was obtained from the gridded cross-calibrated multi-platform (CCMP) wind product with spatial resolution of 0.25° × 0.25°. The CCMP data was produced by combing satellite microwave winds and instrument observations (Atlas et al., 2011). Level 3.0 CCMP V2.0 product was downloaded from the Remote Sensing System (http://www.remss.com/). This product contains surface vector winds at 00:00, 06:00, 12:00, and 18:00. For a specific lake, mean wind of the sampling day was calculated by averaging winds at the four times.

Two scenes of cloud-free OLCI/Sentinel-3A data on 13 and 22 July 2018, covering the MLR-YR region, were downloaded from the European Space Agency Copernicus Open Access Hub (https://scihub.copernicus.eu/). For details about atmospheric correction, algal bloom masking and other preprocessing for the OLCI/Sentinel-3A data, please refer to Shen et al. (2017).

One scene of cloud-free satellite data by MODIS onboard the Terra satellite (MODIS/Terra) on 13 July 2018, covering Lake Taihu (Fig. 1), was downloaded from NASA/Goddard Space Flight Center (GSFC, http://oceancolor.gsfc.nasa.gov). From it, we produced atmospherically Rayleigh-corrected reflectance using the SeaWiFS data analysis system

(SeaDAS, V6.0) by NASA and remote sensing reflectance using the method in Shi et al. (2015b).

### 2.4. Statistic population density and fish catch

Same as Mendonca et al. (2017), the watershed extent of each surveyed lake was identified through the WWF HydroBASINS tool provided by the USGS (www.hydrosheds.org). In the lake watershed extent definition, the HydroSheds dataset was processed with a user-friendly graphical interface. The lake watershed extent was then used to calculate mean population density. In this study, we used gridded population density data in 2010 with spatial resolution of 1000 m × 1000 m from the Global Change Research Data Publishing and Repository System (http://www.geodoi.ac.cn).

We also obtained lake aquaculture area and annual fish catch data in 2012 from the China agricultural statistical yearbook (http://data.stats.gov.cn). Then, we calculated annual fish catch per hectare in different provinces (Fig. 1).

### 2.5. Trophic state index

There are many mathematical methods for assessing lake eutrophication level (Wang et al., 2002 and references therein). For Chinese lakes, we used the trophic state index (TSI) as others (Jin, 1995; Wang et al., 2002; Zhang et al., 2010). The TSI is defined in Eq. (2).

$$\begin{aligned} &\mathrm{TLI} = \sum_{j=1}^{m} W_j \cdot \mathrm{TLI}(j);\ W_j = r_j^2 / \sum_{j=1}^{m} r_j^2 \\ &\mathrm{TLI(TN)} = 10(5.453 + 1.694\ \ln(\mathrm{TN})) \\ &\mathrm{TLI(TP)} = 10(9.436 + 1.624\ \ln(\mathrm{TP})) \\ &\mathrm{TLI(Chl\text{-}a)} = 10(2.5 + 1.086\ \ln(\mathrm{Chl\text{-}a})) \\ &\mathrm{TLI(COD)} = 10(0.109 + 2.66\ \ln(\mathrm{COD})) \\ &\mathrm{TLI(SDD)} = 10(5.118 - 1.94\ \ln(\mathrm{SDD})) \end{aligned} \quad (2)$$

In TSI calculation, TN, TP, Chl-*a*, COD, and SDD were used. Pearson's correlation coefficients ($r_j$) of TN, TP, Chl-*a*, COD, and SDD to Chl-*a* were used to calculate the weight ($W_j$), respectively. With TSI values of <30, 30–50, 50–60, 60–70, and >70, lake was characterized by oligotrophic (O), mesotrophic (M), light eutrophic (lE), middle eutrophic (mE), and hyper eutrophic (hE), respectively (Jin, 1995).

## 3. Results

### 3.1. Aquatic environment scenery

Environment variables of water depth, TN, TP, Chl-*a*, SDD, and COD in the lakes along the MLR-YR covered wide ranges (Fig. 2). Mean ± std of water depth for all surveyed lakes was 1.99 ± 1.01 m in April 2012, but 3.21 ± 1.51 m in August 2012. In April 2012, the maximum TN, TP, Chl-*a*, SDD, and COD were 14.04, 39, 442.95, 20, and 4.72 times of the minimum values, respectively (Fig. 2). In August 2012, the maximum TN, TP, Chl-*a*, SDD, and COD were 7.13, 38, 36.64, 8.85, and 4.26 times of the minimum values, respectively (Fig. 2). On the whole, water quality in August 2012 was worse than that in April 2012.

Eutrophication was the general aquatic environment problem for the lakes along the MLR-YR. In April 2012, the TSI at sampled stations ranged from 31.17 to 75.38, with mean ± std of 52.11 ± 9.49 (Fig. 2f); in August 2012, the TSI at sampled stations ranged from 42.52 to 78.65, with mean ± std of 61.84 ± 8.22 (Fig. 2l). For the 56 surveyed lakes in April 2012, 24 were mesotrophic (M), 19 were light eutrophic (lE), 12 were middle eutrophic (mE), and one was hyper eutrophic (hE) (Fig. 3a, Supplementary Table S1). For the 54 surveyed lakes in August 2012, five were mesotrophic, 17 were light eutrophic, 24 were middle eutrophic, and up to eight were hyper eutrophic (Fig. 3b, Table S1). In general, lake eutrophication along the MLR-YR was time-dependent and more serious in summer.

Lake eutrophication along the MLR-YR was also spatially varying. Most middle- and hyper-eutrophic lakes were located in Hubei and Jiangsu provinces, especially in August 2012 (Fig. 3a, b). For all sampled stations in August 2012, mean ± std of TSI were 65.5 ± 7.56, 52.08 ± 7.91, 58.5 ± 5.8, and 59.16 ± 6.08 in Hubei, Jiangxi, Anhui, and Jiangsu provinces, respectively. It is worth noting that lake eutrophication was

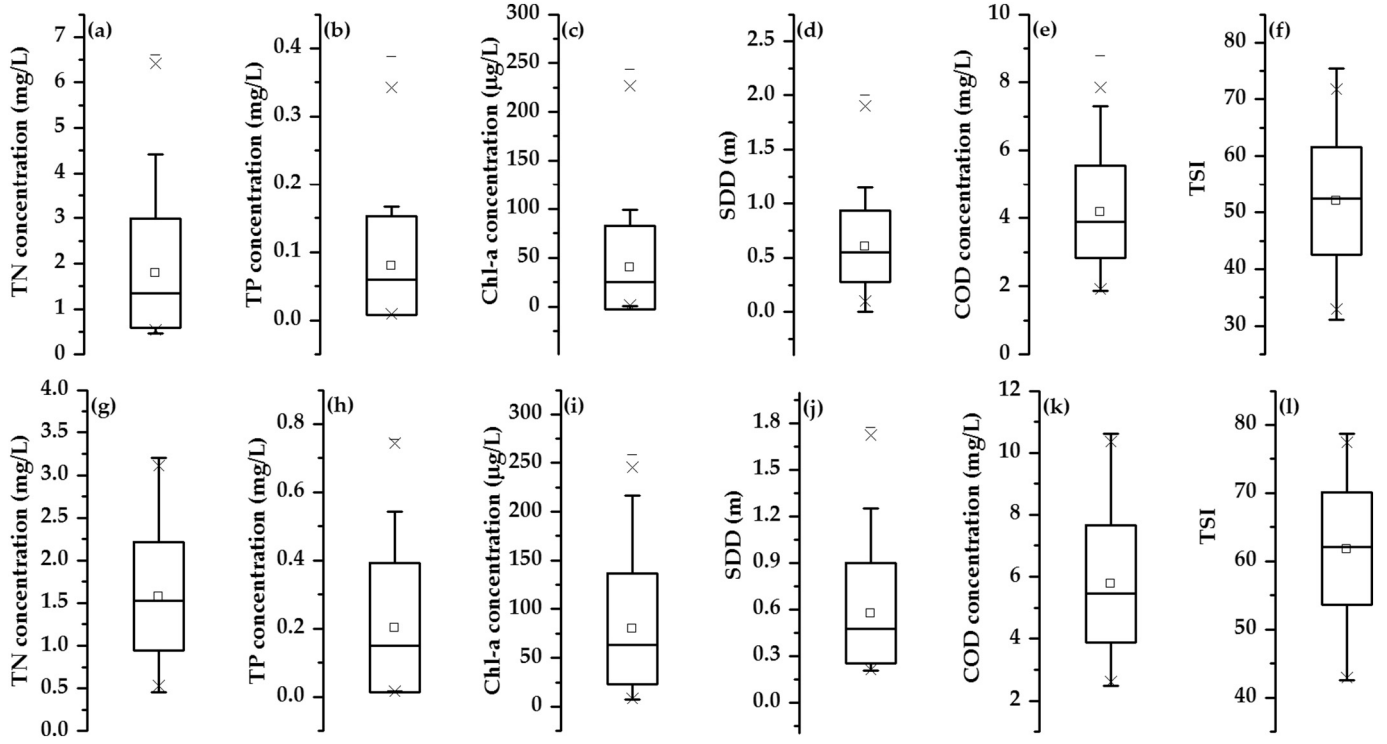


**Fig. 2.** Box-plots of different *in-situ* variables in different seasons: (a) TN, (b) TP, (c) Chl-*a*, (d) SDD, (e) COD, and (f) TSI in April 2012; (g) TN, (h) TP, (i) Chl-*a*, (j) SDD, (k) COD, and (l) TSI in August 2012.

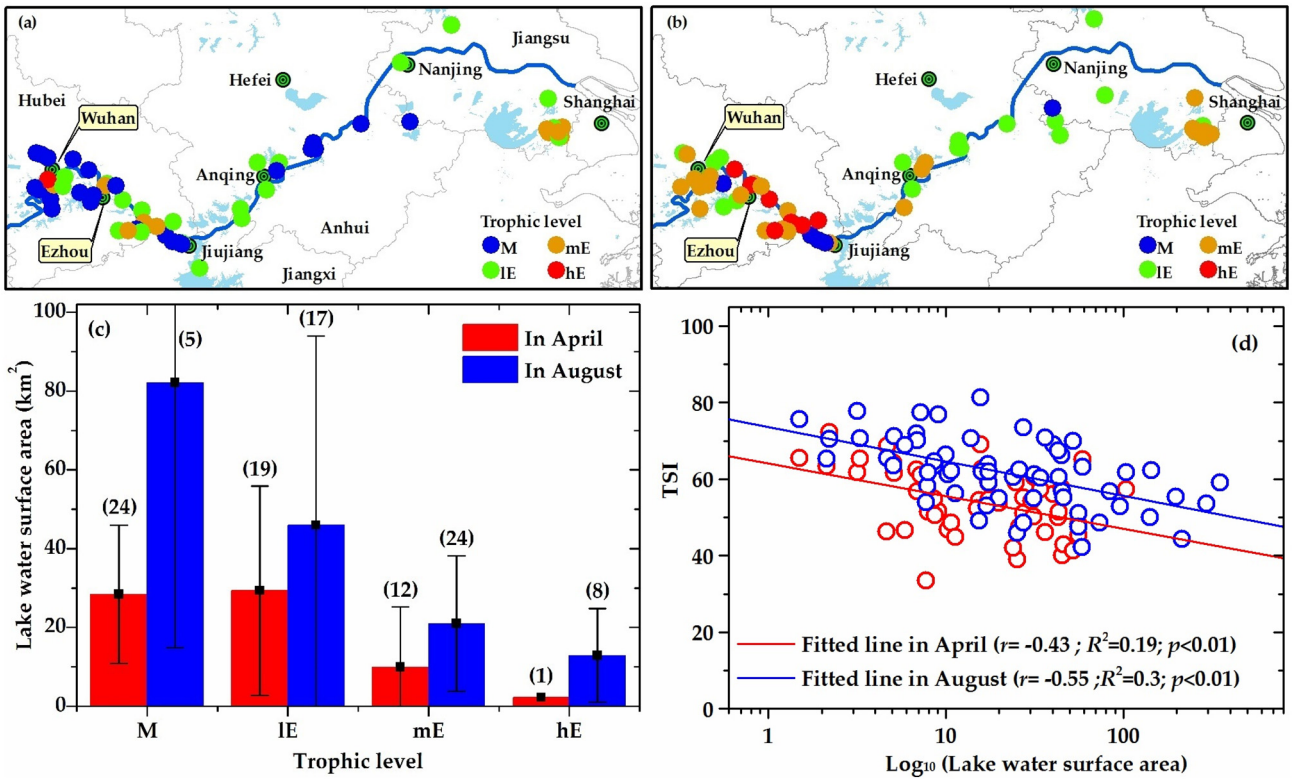


**Fig. 3.** Trophic levels in different lakes and seasons. (a) Trophic levels in April 2012; (b) trophic levels in August 2012; (c) mean lake areas in different trophic levels; (d) linear relationship between TSI and logarithmic lake area. M: mesotrophic lake; lE: light eutrophic lake; mE: middle eutrophic lake; hE: hyper eutrophic lake.

negatively correlated with lake area. With increasing trophic levels, average lake area decreased in both April and August 2012 (Fig. 3c). There was negative linear relationship between TSI and logarithmic lake area in both seasons, with Pearson's $r = -0.43$ ($p < 0.01$, 2-tailed test) in April 2012 and $r = -0.55$ ($p < 0.01$) in August 2012 (Fig. 3d).

### 3.2. Bio-optical properties of suspended particles differed by trophic state

Both SPIM and SPOM concentrations in the lakes along the MLR-YR covered large ranges. In both seasons, *in-situ* SPM ranged from 1.39 to 129.67 mg/L, with mean ± std of 20.35 ± 14.9 mg/L; *in-situ* SPIM ranged from 0.4 to 120.53 mg/L, with mean ± std of 12.92 ± 13.13 mg/L; and *in-situ* SPOM ranged from 0.68 to 23.44 mg/L, with mean ± std of 7.48 ± 4.16 mg/L. Note that SPIM was strongly linearly correlated with SPM ($r = 0.91$ and $p < 0.01$), and determined SPM variation (Fig. 4a). However, both SPIM and SPOM were important components of SPM. For SPM at all *in-situ* stations, SPIM accounted for 56.39 ± 18.73% and SPOM accounted for 43.75 ± 18.65%. SDD in the lakes along the MLR-YR was also co-determined by SPIM and SPOM. There were power relations between SDD and SPIM ($r = 0.86$, $p < 0.01$) and between SDD and SPOM ($r = 0.66$, $p < 0.01$), respectively (Supplementary Fig. S1).

With increasing wavelength λ, $a_d$ exponentially decreased and $a_{ph}$ presented two absorption peaks around 443 and 674 nm (Supplementary Fig. S2). Moreover, phytoplankton absorption coefficient at 443 nm ($a_{ph}(443)$) was generally higher than that at 674 nm ($a_{ph}(674)$) (Fig. S2). Hence, $a_{ph}(443)$ and NAP absorption coefficient at 443 nm ($a_d(443)$) were used to study optical properties of suspended particles in the lakes along the MLR-YR. There were strong linear correlations between absorption coefficients ($a_d(443)$ and $a_{ph}(443)$) and suspended particulate concentrations (SPIM and SPOM); $a_d(443)$ was strongly correlated with SPIM, with $r = 0.73$ and $p < 0.01$ (Fig. 4c); and $a_{ph}(443)$ was strongly correlated with SPOM, with $r = 0.76$ and $p < 0.01$ (Fig. 4d). Therefore, the same as SPIM and SPOM concentrations, $a_d(443)$ and $a_{ph}(443)$ also covered wide ranges. Moreover, both $a_d^*(443)$ and $a_{ph}^*(443)$ decreased with increasing SPIM and Chl-*a*, respectively (Fig. 5a). Both *r* between $a_d^*(443)$ and SPIM and between $a_{ph}^*(443)$ and Chl-*a* generally increased from 400 to 700 nm (Fig. 5b).

Although with wide ranges, bio-optical properties of suspended particles in the lakes along the MLR-YR could be quantitatively described by the TSI. All SPIM, SPOM, $a_d(443)$, and $a_{ph}(443)$ generally increased with increasing trophic levels from mesotrophic to light eutrophic, to middle eutrophic, and further to hyper eutrophic in both April and August 2012. With increasing trophic levels, for example, mean ± std of $a_{ph}(443)$ was 0.53 ± 0.25 $m^{-1}$, 1.43 ± 0.77 $m^{-1}$, 3.11 ± 1.53 $m^{-1}$, and 5.05 ± 0.82 $m^{-1}$ in August 2012 for mesotrophic, light eutrophic, middle eutrophic, and hyper eutrophic lakes, respectively. For all *in-situ* stations ($N = 332$), both $a_d(443)$ and $a_{ph}(443)$ were exponentially related to TSI, especially $a_{ph}(443)$; for $a_d(443)$, $r = 0.5$ ($p < 0.01$); and for $a_{ph}(443)$, $r = 0.83$ ($p < 0.01$) (Fig. 4b).

### 3.3. Tempo-spatial variation of bio-optical compositions

Suspended particulate compositions in the lakes along the MLR-YR varied tempo-spatially. For different provinces from upstream to downstream, both mean SPIM and SPOM concentrations increased in April 2012 (Fig. 6a, d). Mean SPIM was 8.43 ± 7.22, 9.39 ± 6.5, 15.7 ± 19.9, and 17.07 ± 11.47 mg/L in Hubei, Jiangxi, Anhui, and Jiangsu provinces, respectively (Fig. 6a); mean SPOM was 6.04 ± 3.66, 6.77 ± 1.49, 7.25 ± 3.27, and 8.03 ± 1.43 mg/L, respectively (Fig. 6d). However, both mean SPIM and SPOM concentrations had high values in Hubei and Jiangsu provinces, but low values in Jiangxi and Anhui provinces in August 2012 (Fig. 6a, d). Mean SPIM was 12.22 ± 9.29, 7.03 ± 3.49, 9.96 ± 8.07, and 16.44 ± 11.42 mg/L in Hubei, Jiangxi, Anhui, and Jiangsu provinces, respectively (Fig. 6a); mean SPOM was 10.36 ± 4.69, 3.74 ± 1.81, 4.14 ± 2.32, and 6.3 ± 3.93 mg/L, respectively (Fig. 6d).

Due to the strong linear relationships between $a_d(443)$ and SPIM (Fig. 4c) and between $a_{ph}(443)$ and SPOM (Fig. 4d), $a_d(443)$ and

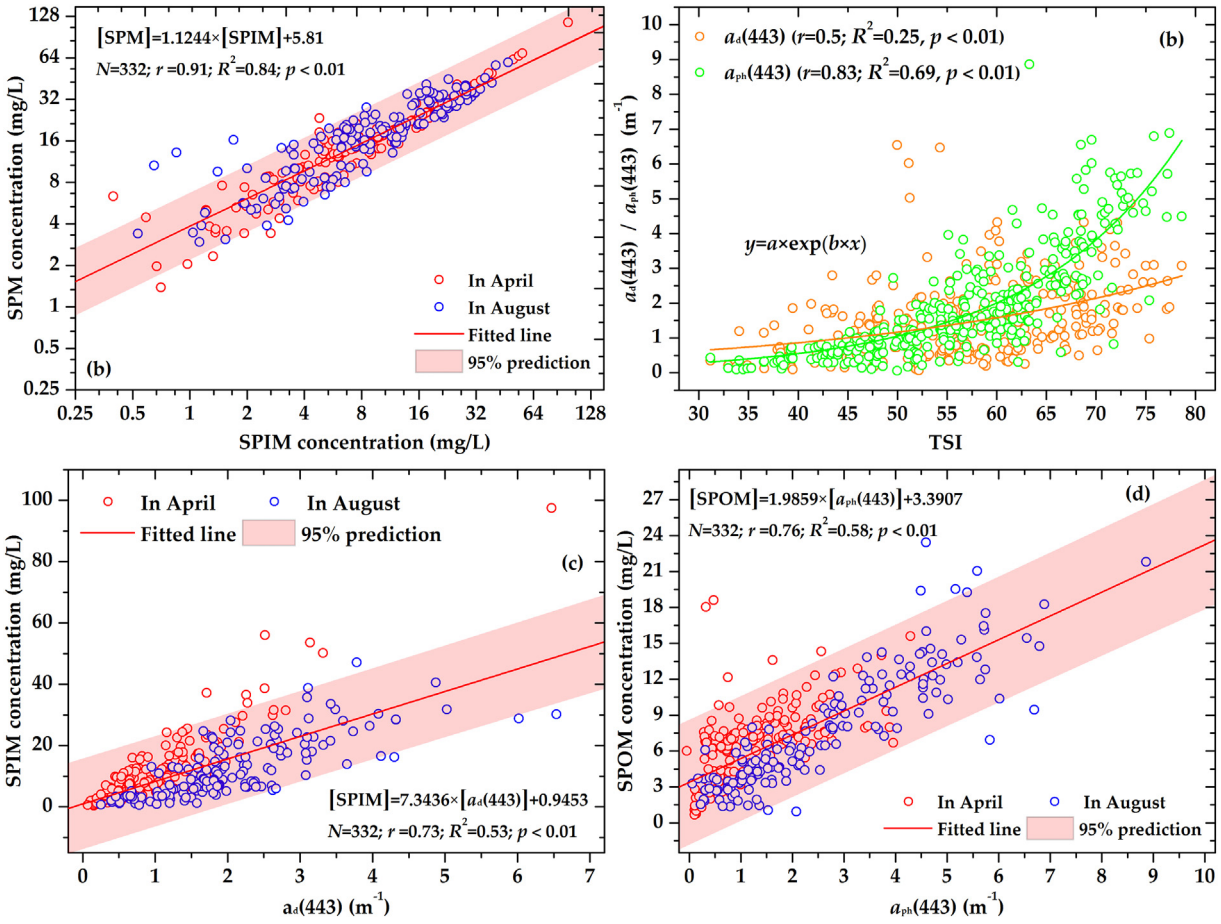


**Fig. 4.** Relationships between different bio-optical variables of suspended particles: (a) between SPM and SPIM; (b) between optical properties ($a_d(443)$ and $a_{ph}(443)$) and TSI; (c) between SPIM and $a_d(443)$; (d) between SPOM and $a_{ph}(443)$. In the curve fittings, all paired *in-situ* data ($N = 332$) was used.

$a_{ph}(443)$ showed similar spatial distributions as SPIM and SPOM, respectively. More specifically, most lakes with high $a_d(443)$ and $a_{ph}(443)$ were distributed in Hubei and Jiangsu provinces, especially around large cities such as Wuhan and Shanghai (Fig. 6). Almost all sampled lakes around the Shanghai metropolis were characterized by high $a_d(443)$ and $a_{ph}(443)$ (Fig. 6). On the contrary, the lakes far from cities were usually characterized by low $a_d(443)$ and $a_{ph}(443)$ (Fig. 6).

## 4. Discussion

### 4.1. Impact factors on SPM compositions

The MLR-YR region is of international interest. First, it is one of the most developed regions in China and has intensive human activities (Cao et al., 2017; Feng et al., 2012; Zhang et al., 2019). Second, it

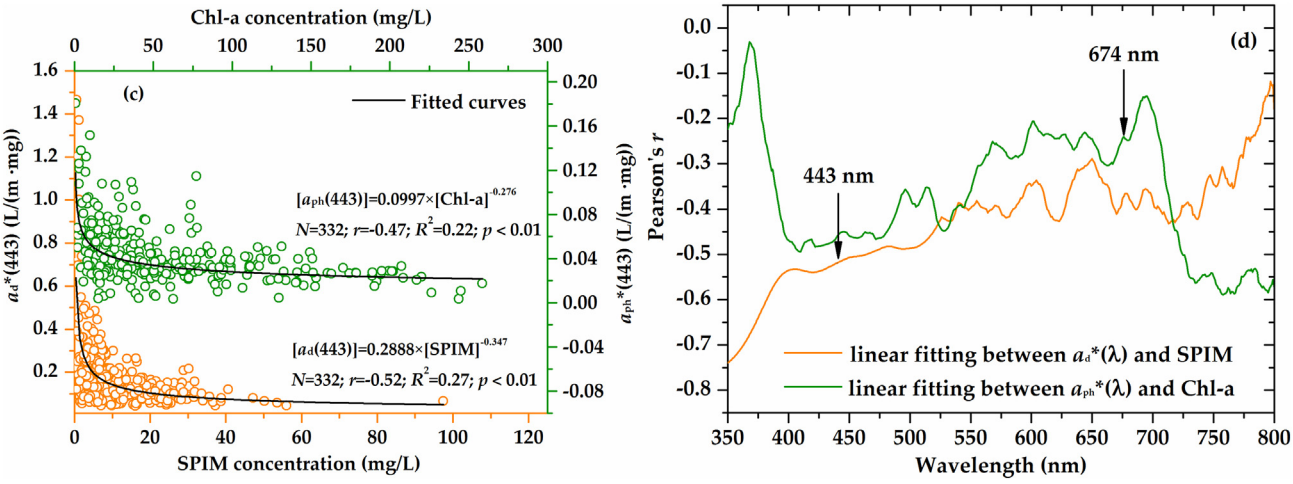


**Fig. 5.** Package effects of SPIM and phytoplankton. (a) The power functions between $a_d^*(440)$ and SPIM and between $a_{ph}^*(443)$ and Chl-*a*. (b) The Pearson's *r* of the power functions at different wavelengths.

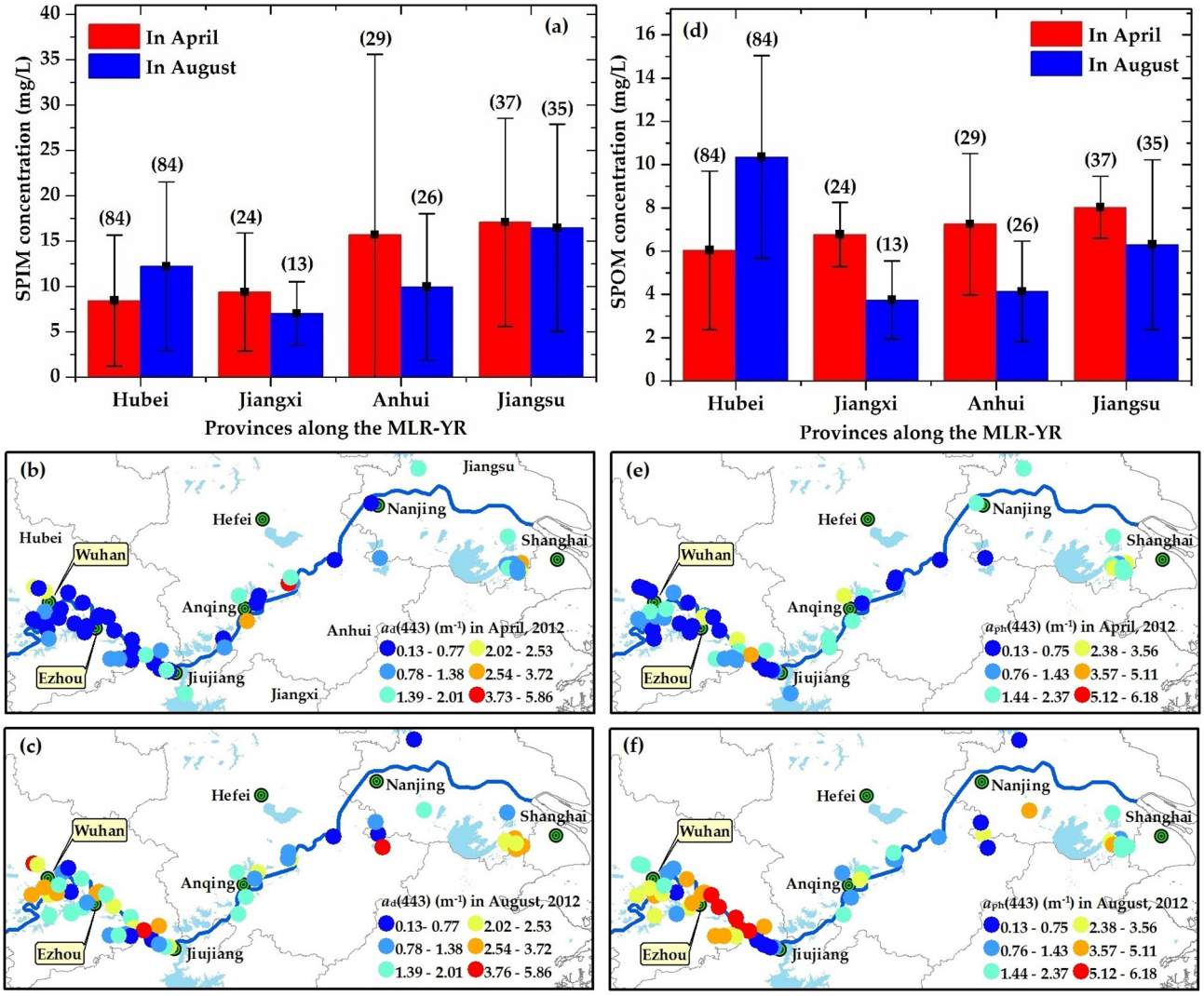


**Fig. 6.** Tempo-spatial distributions of bio-optical properties of suspended particles. (a) and (d) are mean SPIM and SPOM concentrations in different provinces, respectively. The filled rectangle denotes mean value and the error line denotes standard deviation. Digitals in brackets denote *in-situ* sample size. (b) and (c) are mean *in-situ* $a_d(443)$ in April and August 2012, respectively. (e) and (f) are mean *in-situ* $a_{ph}(443)$ in April and August 2012, respectively. For geographic information, please refer to Fig. 1.

contains numerous lakes and is an ideal area for studying various lakes in a group (Hou et al., 2017; Ma et al., 2010; Wang et al., 2014). Third, it not only contains turbid lakes with high suspended sediment concentrations (the Lake Hongze and Lake Poyang, for examples), but also includes eutrophic lakes with high phytoplankton production (the Lake Taihu and Lake Chaohu, for instances) (Cao et al., 2017; Duan et al., 2017; Feng et al., 2011, 2012; Hou et al., 2017).

Bio-optical properties in lakes are influenced by both human activities and climatic factors (Duan et al., 2014, 2017; Feng et al., 2012; Hou et al., 2017; Zhang et al., 2016). Being influenced by different human-induced factors (population density in Supplementary Fig. S3 for example) and climatic factors (wind speed along with increasing longitude in Supplementary Fig. S4 for instance), bio-optical properties in different lakes varied greatly tempo-spatially and resulted in large standard deviations (Section 3). Although SPIM explained 91% of SPM variation (Fig. 4a), SPM compositions at different stations varied greatly. For all *in-situ* stations, mass percent of SPOM in SPM ranged from 15.62% to 93.76% in April 2012, and from 7.88% to 93.87% in August 2012. For the eutrophic shallow lakes along the MLR-YR, phytoplankton production and sediment resuspension were two important SPM sources (Kong and Gao, 2005; Markensten and Pierson, 2003; Zhang et al., 2006).

*4.1.1. Human-induced eutrophication*

Lake eutrophication varied spatially due to human activities. Population density in Jiangsu Province was significantly higher than those in the other three provinces (Supplementary Fig. S3). Moreover, lake aquaculture was the most active in Hubei and Jiangsu provinces. In 2012, annual fish catch per unit area was 5.41, 4.87, 3.15, and 5.45 tons per hectare in Hubei, Jiangxi, Anhui, and Jiangsu provinces, respectively (Section 2.4). As a result, TSI and bio-optical properties of suspended particles showed high values in Hubei and Jiangsu provinces, but low values in Jiangxi and Anhui provinces in August 2012 (Figs. 3, 6).

Human-induced eutrophication increased phytoplankton production. Human activities were primarily responsible for eutrophication and phytoplankton bloom in the lakes along the MLR-YR (Jin, 1995). Human activities including agricultural fertilizing (Bennett et al., 2001; Sharpley and Meyer, 1994), sewage discharge (Paerl et al., 2011), aquaculture (Guo and Li, 2003) would increase lake TN and TP concentrations. Both TN and TP were important factors impacting phytoplankton production. TN was moderately linearly related to Chl-*a*, with $r = 0.48$ ($p < 0.01$) in April 2012 and $r = 0.6$ ($p < 0.01$) in August 2012 (Fig. 7a). TP was also moderately linearly related to Chl-*a*, with $r = 0.69$ ($p < 0.01$) in April 2012 and $r = 0.61$ ($p < 0.01$) in August 2012 (Fig. 7b). For Lake Taihu, Ai et al. (2014) reported that phosphorus was the key factor for regulating phytoplankton community structure and that nitrogen was important for

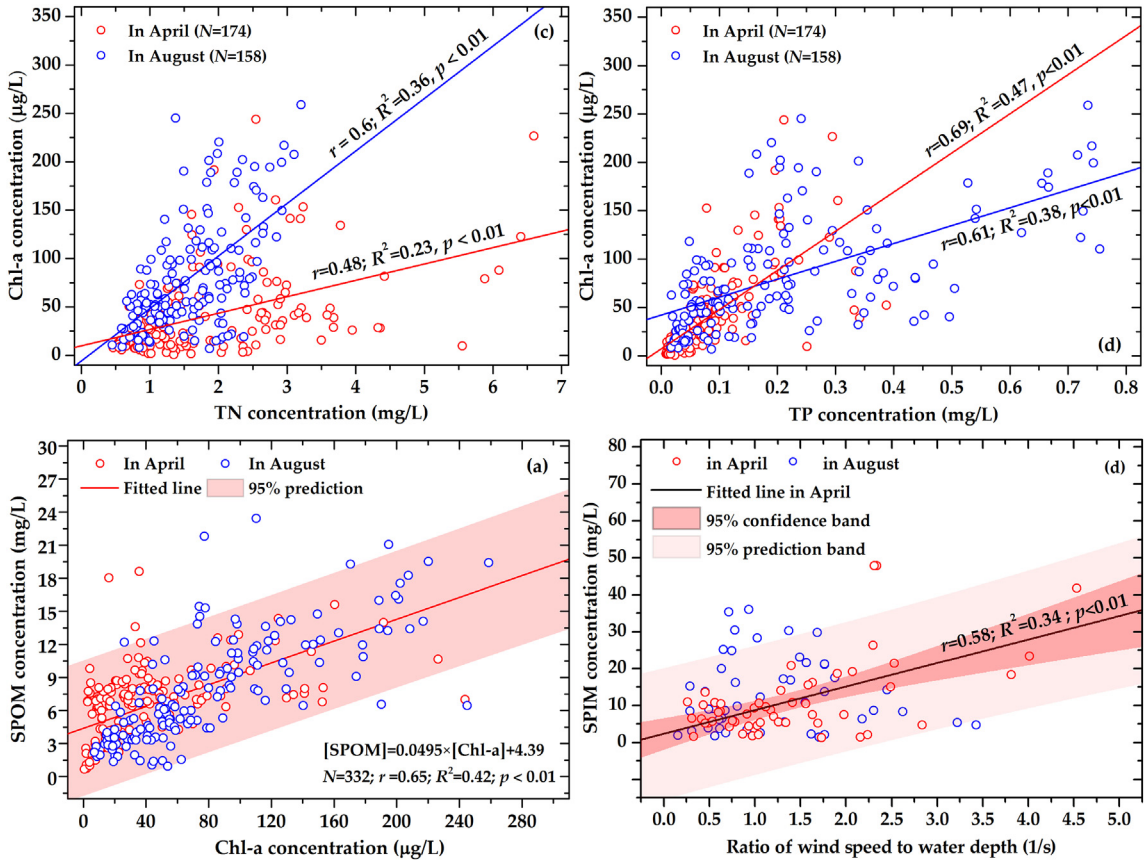


**Fig. 7.** Impact factors on suspended particulate compositions. (a) and (b) show the influences of TN and TP on phytoplankton production, respectively. (c) and (d) show the impacts of phytoplankton production and wind speed on SPOM and SPIM concentrations, respectively. Mean wind speed on the sampling day was calculated by averaging wind speeds at 00:00, 06:00, 12:00, and 18:00 from the Level 3.0 CCMP V2.0 product (Section 2.3).

phytoplankton distribution. Therefore, to control phytoplankton production, it is necessary to manage both TN and TP from human activities (Paerl et al., 2011; Xu et al., 2010).

Phytoplankton production was an important SPOM source for the lakes along the MLR-YR. Compared with only 1.04 ± 1.07 μg/L of Chl-*a* in oligotrophic Yungui Plateau lakes (Zhang et al., 2010), Chl-*a* was higher in the lakes along the MLR-YR (Fig. 2c, i). With $R^2 = 0.42$ ($p < 0.01$) for the linear relationship between SPOM and Chl-*a*, phytoplankton production could explain 42% of SPOM variation (Fig. 7c). From the linear fitting slope, we further derived that phytoplankton with 1 μg of Chl-*a* contained 0.0495 mg of SPOM (Fig. 7c). Wang and Wang (1984) reported that phytoplankton with 1 μg of Chl-*a* contained a total of 0.862 mg of wet biomass in Lake Wuhandong, one of the lakes in our study (Fig. 1, Table S1). By using the ratio of dry biomass to wet biomass as 0.1 (Bum and Pick, 1996), we deduced that phytoplankton with 1 μg of Chl-*a* contained a total of 86.2 μg of dry biomass, namely, the total SPM. Based on the above reasoning, we estimated that phytoplankton production contributed 18.42 ± 18.92% of SPIM and 26.22 ± 19.24% of SPOM in April 2012, but 30.4 ± 23.41% of SPIM and 47.03 ± 18.1% of SPOM in August 2012.

To quantitatively describe contributions of different drivers to suspended particulate compositions, multiple general linear model (GLM) regression was performed. Multiple GLM was often used to explore possible contributions of impact factors (Tao et al., 2015; Tong et al., 2017). From the multiple GLM results, we observed that TSI explained 42.84% of SPOM variation in April 2012, and 54.64% in August 2012 (Table 1).

*4.1.2. Wind-induced sediment resuspension*

Wind also has important impacts on suspended particulate compositions. Chl-*a* was 40.12 ± 42.42 μg/L in April 2012, but 80.04 ± 56.78 μg/L in August 2012 (Fig. 2c, i). With lower impacts by phytoplankton production in April 2012, both SPIM and SPOM had similar spatial distributions as mean wind speed on the sampling day, which generally increased from upstream to downstream (Fig. 6, Supplementary Fig. S4). From the multiple GLM results, we observed that wind had significant effects on SPIM ($p < 0.05$) and explained 9.36% of SPIM variation in April 2012 (Table 1).

Wind can intensify sediment resuspension, which plays an important role in the variation of SPM in shallow lakes (Giardino et al., 2013; Qin, 2004; Xue et al., 2015), but water depth can weaken wind's effects on sediment resuspension. In this study, we used the ratio of wind speed to water depth (wind/depth) to discuss wind's effects on sediment resuspension. Sediment is featured by high SPIM fraction and low SPOM fraction; for example, organic matter content in sediment was only 4.0% in Lake Taihu (Qin, 2004). In these cases,

**Table 1**
Multiple GLM results of the relationships between impact factors and suspended particulate compositions in April and August 2012. Pop: population density in lake watershed; MS: mean squares; SS: proportion of variances explained by the variable.

| Variables | SPIM in April | | SPOM in April | | SPIM in August | | SPOM in August | |
|---|---|---|---|---|---|---|---|---|
| | MS | SS (%) | MS | SS (%) | MS | SS (%) | MS | SS (%) |
| TSI | 358.21* | 5.79 | 203.73** | 42.84 | 219.97* | 5.01 | 535.21** | 54.64 |
| Pop | 333.04* | 5.39 | 0.42 | 0.09 | 7.17 | 0.16 | 0.01 | 0.01 |
| Wind | 578.87** | 9.36 | 0.01 | 0.01 | 187.17 | 4.26 | 0.05 | 0.01 |
| Area | 130.35 | 2.11 | 16.41* | 3.45 | 89.71 | 2.04 | 15.05 | 1.54 |
| Depth | 221.04 | 3.57 | 5.57 | 1.17 | 122.32 | 2.79 | 4.89 | 0.5 |
| Residuals | 4562.52 | 73.78 | 249.46 | 52.45 | 3763.01 | 85.73 | 424.29 | 43.32 |

* $p < 0.1$.
** $p < 0.05$.

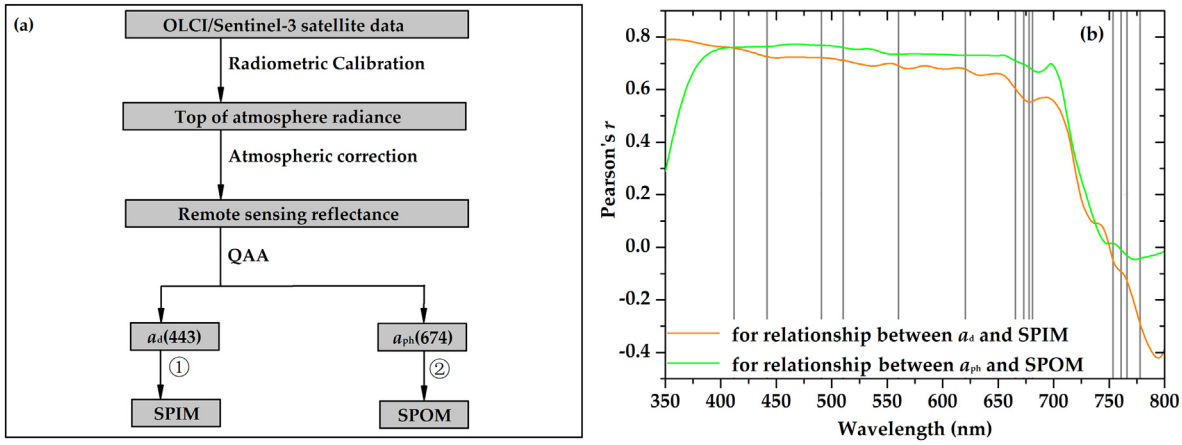


**Fig. 8.** (a) Recommended flowchart for monitoring SPM compositions using satellite data. ① and ② are linear equations between $a_d$(443) and SPIM (Fig. 4c) and between $a_{ph}$(674) and SPOM, respectively. (b) Pearson's *r* between $a_d$(443) and SPIM and between $a_{ph}$(674) and SPOM at different wavelengths. Gray lines show the central wavelengths of OLCI/Sentinel-3A data.

SPIM was moderately positively related to the wind/depth ratio in April 2012, with $r = 0.58$ and $p < 0.01$ (Fig. 7d). However, no significant relationship between SPIM and the wind/depth ratio was found in August 2012 (Fig. 7d). It might be because that wind was not strong enough in August. For all sampled lakes in August 2012, mean ± std of wind speed was only 2.98 ± 1.42 m/s. For the shallow Lake Markermeer in the central Netherlands, Eleveld (2012) reported that sediment resuspension was not significant under low wind speed (≤ 3 m/s). Moreover, water depth in August (3.21 ± 1.51 m) was deeper than that in April 2012 (1.99 ± 1.01 m) in this study.

### 4.2. Implications for remote sensing of SPM compositions

#### 4.2.1. Recommended framework

We recommend the OCLI/Sentinel-3 data. With full spatial resolution of 300 m × 300 m, OLCI is suitable for monitoring various small lakes along the MLR-YR (Table S1). The Sentinel-3A and -3B form a two-satellite monitoring network, which provides observations of the Earth once every 1.5 days (Shen et al., 2017). With Sentinel-3C and -3D, higher temporal resolution data for monitoring lakes will be achievable (Section 1). High tempo-spatial resolution of OLCI/Sentinel-3 data was

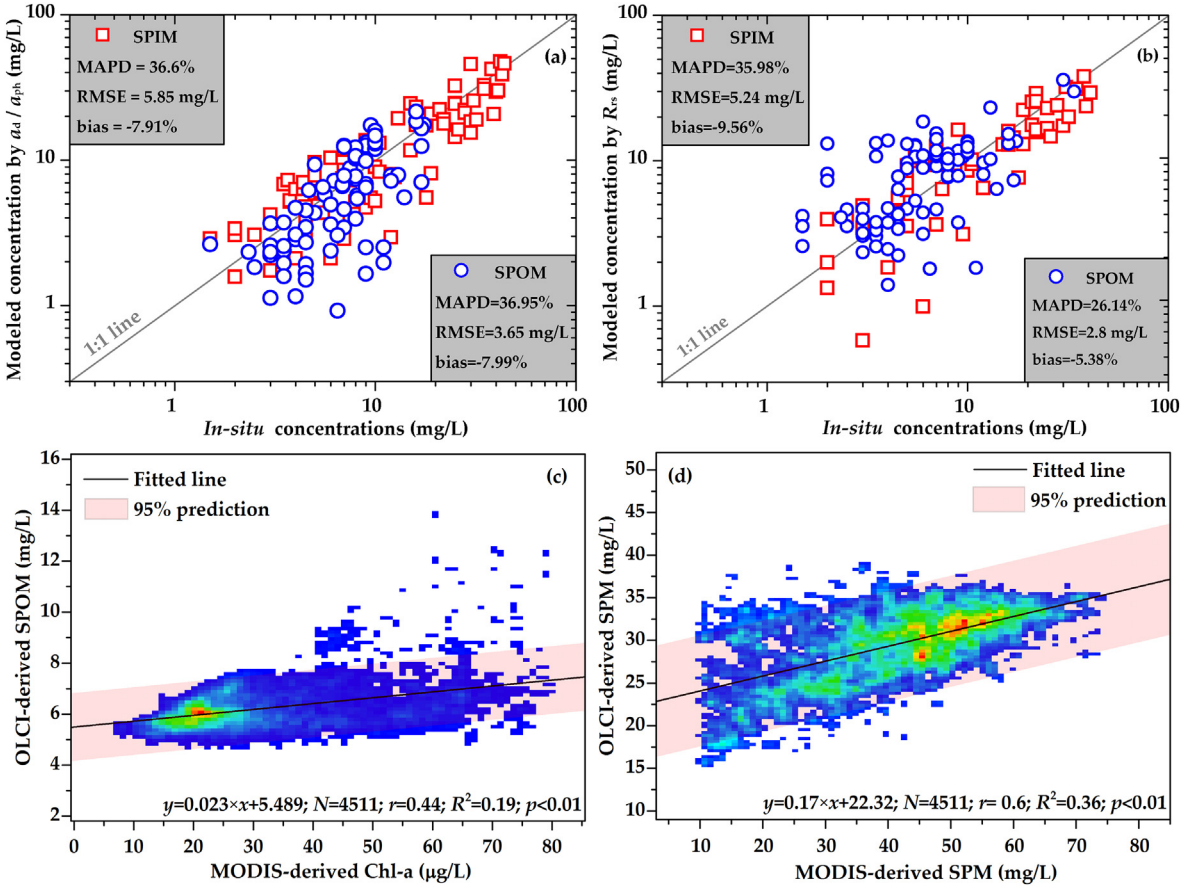


**Fig. 9.** Validations of the modeled results. (a) For modeled SPIM and SPOM concentrations by *in-situ* $a_d$(443) and $a_{ph}$(674). (b) For modeled SPIM and SPOM concentrations by *in-situ* $R_{rs}$. (c) The relationship between OLCI-derived SPOM and MODIS-derived Chl-*a*. (d) The relationship between OLCI-derived SPM and MODIS-derived SPM.

recommended for monitoring high tempo-spatially varied eutrophic shallow lakes (Section 3).

For retrieving SPM compositions, we recommend two-step algorithms. The green, red, and near-infrared bands are able to characterize the scattering properties of suspended particles, so they are usually used to derive SPM (Feng et al., 2012; Hou et al., 2017; Petus et al., 2010; Shi et al., 2015b). However, both scattering spectra of SPIM and SPOM follow wavelength-dependent power-law function (Lyu et al., 2015), so it is hard to differentiate them by using their scattering properties. Based on the linear relationships between absorption properties and SPM compositions (Fig. 4c, d), the absorption properties are good choices. Moreover, two-step processes allow for identifying appropriate algorithms for material with complex source variations (Jiang et al., 2015). Therefore, we recommend the framework for retrieving SPM compositions as shown in Fig. 8a.

*4.2.2. Rationality and feasibility*

In practice, $a_d(443)$ and $a_{ph}(674)$ are recommended. Both SPIM and phytoplankton have package effects, which mean specific light absorption efficiency and should be calculated by dividing their light absorption coefficients by concentrations, respectively (Nelson et al., 1993; Xue et al., 2017). Because of package effects, increased SPIM and Chl-*a* led to decreases in $a_{d^*}$ and $a_{ph^*}$ (Fig. 5a). Pearson's *r* between $a_{ph}$ and SPOM did not show great difference from 400 to 700 nm (Fig. 8b), but phytoplankton had strong absorption (Fig. S2b) and weak package effect at 674 nm (Fig. 5b). Therefore, $a_{ph}(674)$ is recommended as other studies did (Ma et al., 2006; Oubelkheir et al., 2005; Shi et al., 2013). Although SPIM also had strong package effects at short wavelengths, both SPIM's absorption (Fig. S2) and Pearson's *r* between $a_d$ and SPIM decreased from 400 to 700 nm (Fig. 8b). To better distinguish $a_d$ and $a_{ph}$, $a_d(443)$ is recommended as other studies did (Shi et al., 2013; Xue et al., 2017; Ylöstalo et al., 2014).

Both $a_d(443)$ and $a_{ph}(674)$ are optical variables, which can be derived from remote sensing data using semi-analytical algorithms. Although the commonly used semi-analytical algorithms were developed for ocean Case-I waters, they could be applied to inland Case-II waters after local calibration, for example the QAA (Wang et al., 2009). The semi-analytical algorithms developed for retrieving $a_{ph}$ in eutrophic inland waters by Gons et al. (2002) and Simis et al. (2005) were reported to be applicable to Lake Chaohu and Lake Taihu after local calibration (Wu et al., 2015). Then, using the linear relationships between suspended particulate compositions and related optical properties

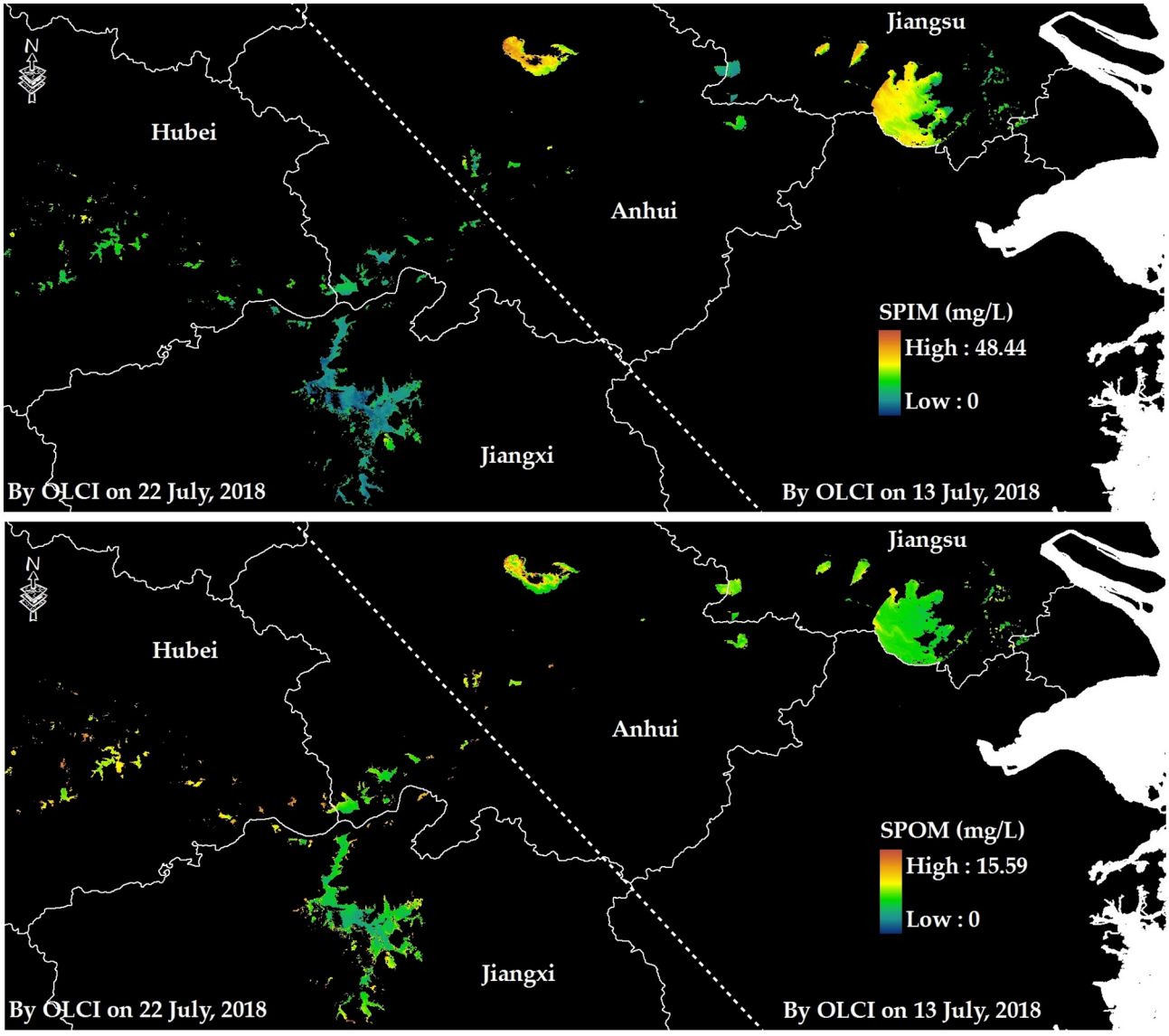


**Fig. 10.** Satellite-derived SPIM and SPOM concentrations in lakes along the MLR-YR. Two scenes of OLCI/Sentinel-3A data on 20 and 13 July 2018 were used. For spatial distributions of different lakes, please refer to Fig. 1.

(Fig. 4c, d), we could further calculate SPIM and SPOM concentrations, respectively.

For the lakes along the MLR-YR, SPIM was strongly linearly related to $a_d(443)$ (Fig. 4c), and SPOM was strongly linearly related to $a_{ph}(674)$ ([SPOM] = 3.5 × $a_{ph}(674)$ + 3.97, $r = 0.79$; $R^2 = 0.59$, $p < 0.01$). Using the *in-situ* data collected in August 2018 (Section 2.2.3), modeled results were validated (Fig. 9a). For modeled SPIM using *in-situ* $a_d(443)$, mean absolute percent difference (MAPD) was 36.6%; root mean square error (RMSE) was 5.85 mg/L, and bias was −7.91% (Fig. 9a). For modeled SPOM using *in-situ* $a_{ph}(674)$, MAPD, RMSE, and bias were 36.95%, 3.65 mg/L, and −7.99%, respectively (Fig. 9a). The MAPD, RMSE, and bias were defined as in Cao et al. (2018). On the whole, the modeled SPIM and SPOM using *in-situ* $a_d(443)$ and $a_{ph}(674)$ were acceptable.

*4.2.3. Application examples*

For the lakes along the MLR-YR, a modified QAA proposed by Lee et al. (2002) was used to derive $a_d(443)$ and $a_{ph}(674)$ from $R_{rs}$. From the *in-situ* $R_{rs}$ in August 2018 (Section 2.2.3), SPIM and SPOM concentrations were estimated. Validation results are shown in Fig. 9b. For modeled SPIM, MAPD, RMSE, and bias were 35.98%, 5.24 mg/L, and −9.56%, respectively (Fig. 9b). For modeled SPOM, MAPD, RMSE, and bias were 26.14%, 2.8 mg/L, and −5.38%, respectively (Fig. 9b). These modeled results using *in-situ* $R_{rs}$ were also acceptable.

The recommended flowchart was also applied to OLCI-derived $R_{rs}$ by using OLCI/Sentinel-3A data (Fig. 10). Spatial distributions of OLCI-derived SPIM and SPOM were similar to the *in-situ* results in August 2012, with high values in Hubei Province and low values in Jiangxi Province (Figs. 6, 10). Mean ± std of OLCI-derived SPOM (8.86 ± 2.14 mg/L) was close to the *in-situ* results in August 2012 (7.89 ± 4.88 mg/L). However, mean ± std of OLCI-derived SPIM (21.77 ± 6.61 mg/L) was significantly higher than the *in-situ* values in August 2012 (12.36 ± 9.67 mg/L). Two typhoons, *Maria* and *Ampil*, passed through the MLR-YR on 12 and 22 July 2018, respectively (http://agora.ex.nii.ac.jp/). High SPIM in July 2018 might due to strong wind-induced sediment resuspension.

For the lakes along the MLR-YR, SPOM was linearly related to Chl-*a*, with $p < 0.01$ (Fig. 7c). Due to no available *in-situ* data for validating OLCI-derived SPIM and SPOM (Fig. 10), we compared them with Chl-*a* and SPM derived by MODIS/Terra data. On 13 July 2018, MODIS/Terra scanned Lake Taihu. We derived Chl-*a* and SPM from the MODIS/Terra data using the local algorithms proposed by Shi et al. (2015a) and Shi et al. (2015b), respectively. The comparison of results is shown in Fig. 10. OLCI-derived SPOM was correlated with MODIS-derived Chl-*a*, with $r = 0.44$ and $p < 0.01$ (Fig. 9c). OLCI-derived SPM was also correlated with MODIS-derived SPM, with $r = 0.6$ and $p < 0.01$ (Fig. 9d). The low $r$ values might be due to atmospheric correction error in obtaining accurate remote sensing reflectance for inland water (IOCCG, 2000). However, these linear relationships indicated the proposed flowchart mat be used to derive SPM compositions from space.

## 5. Conclusions

The shallow lakes along the MLR-YR were characterized as seriously eutrophic. For the surveyed 59 lakes in both dry and wet seasons in 2012, none were oligotrophic. In these cases, bio-optical compositions of SPM were differed by trophic state index, and generally showed high values for lakes influenced by strong human activities. For the eutrophic shallow lakes, significant tempo-spatial variation of SPM compositions was dominated by human-induced eutrophication. In the dry season with low phytoplankton production, wind-induced sediment resuspension also had significant impacts on SPM compositions. Moreover, based on the strong relationships between optical properties and SPM compositions, SPM compositions in the lakes along the MLR-YR could be derived from OLCI/Sentinel-3 satellite data.

## Acknowledgement

This study was supported by the Strategic Priority Research Program of the Chinese Academy of Sciences (Grant #XDA19040500), National Natural Science Foundation of China (Grants #41671358 and #41431176), the Research Startup Project of Nanjing Institute of Geography and Limnology, Chinese Academy of Sciences (Grant #Y7SL051001), and the Natural Science Foundation of Jiangsu Province (Grants #BK20181102 and #BK20160049).

## Appendix A. Supplementary data

Supplementary data to this article can be found online at https://doi.org/10.1016/j.scitotenv.2019.02.366.

## References

Ai, Y., Bi, Y., Hu, Z., 2014. Changes in phytoplankton communities along nutrient gradients in Lake Taihu: evidence for nutrient reduction strategies. Chin. J. Oceanol. Limnol. 33, 447–457.
APHA, 1995. Standard Methods for the Examination of Water and Wastewater. 19th edition. American Public Health Association, Washington, D. C.
Atlas, R., Hoffman, R.N., Ardizzone, J., Leidner, S.M., Jusem, J.C., Smith, D.K., Gombos, D., 2011. A cross-calibrated, multiplatform ocean surface wind velocity product for meteorological and oceanographic applications. Bull. Am. Meteorol. Soc. 92, 157–174.
Bennett, E.M., Carpenter, S.R., Caraco, N.F., 2001. Human impact on erodable phosphorus and eutrophication: a global perspective. Bioscience 51, 227–234.
Bricaud, A., Morel, A., Babin, M., Allali, K., Claustre, H., 1998. Variations of light absorption by suspended particles with chlorophyll a concentration in oceanic (case 1) waters: analysis and implications for bio-optical models. Journal of Geophysical Research: Oceans 103, 31033–31044.
Bricaud, A., Babin, M., Claustre, H., Ras, J., Tièche, F., 2010. Light absorption properties and absorption budget of Southeast Pacific waters. J. Geophys. Res.: Oceans 115.
Bum, B.K., Pick, F.R., 1996. Factors regulating phytoplankton and zooplankton biomass in temperate rivers. Limnology & Oceanography 41, 1572–1577.
Cao, Z., Duan, H., Feng, L., Ma, R., Xue, K., 2017. Climate-and human-induced changes in suspended particulate matter over Lake Hongze on short and long timescales. Remote Sens. Environ. 192, 98–113.
Cao, F., Tzortziou, M., Hu, C., Mannino, A., Fichot, C.G., Del Vecchio, R., Najjar, R.G., Novak, M., 2018. Remote sensing retrievals of colored dissolved organic matter and dissolved organic carbon dynamics in North American estuaries and their margins. Remote Sens. Environ. 205, 151–165.
Cleveland, J.S., Weidemann, A.D., 1993. Quantifying absorption by aquatic particles: a multiple scattering correction for glass-fiber filters. Limnology & Oceanography 38, 1321–1327.
Duan, H.T., Ma, R.H., Xu, X.F., Kong, F.X., Zhang, S.X., Kong, W.J., Hao, J.Y., Shang, L.L., 2009a. Two-decade reconstruction of algal blooms in China's Lake Taihu. Environmental Science & Technology 43, 3522–3528.
Duan, H.T., Ma, R.H., Zhang, Y.Z., Zhang, B., 2009b. Remote-sensing assessment of regional inland lake water clarity in northeast China. Limnology 10, 135–141.
Duan, H., Feng, L., Ma, R., Zhang, Y., Arthur Loiselle, S., 2014. Variability of particulate organic carbon in inland waters observed from MODIS Aqua imagery. Environ. Res. Lett. 9, 084011.
Duan, H., Tao, M., Loiselle, S.A., Zhao, W., Cao, Z., Ma, R., Tang, X., 2017. MODIS observations of cyanobacterial risks in a eutrophic lake: implications for long-term safety evaluation in drinking-water source. Water Res. 122, 455–470.
Eleveld, M.A., 2012. Wind-induced resuspension in a shallow lake from Medium Resolution Imaging Spectrometer (MERIS) full-resolution reflectances. Water Resour. Res. 48.
Feng, L., Hu, C., Chen, X., Li, R., Tian, L., Murch, B., 2011. MODIS observations of the bottom topography and its inter-annual variability of Poyang Lake. Remote Sens. Environ. 115, 2729–2741.
Feng, L., Hu, C., Chen, X., Tian, L., Chen, L., 2012. Human induced turbidity changes in Poyang Lake between 2000 and 2010: observations from MODIS. Journal of Geophysical Research: Oceans 117.
Gernez, P., Barillé, L., Lerouxel, A., Mazeran, C., Lucas, A., Doxaran, D., 2014. Remote sensing of suspended particulate matter in turbid oyster-farming ecosystems. Journal of Geophysical Research: Oceans 119, 7277–7294.
Giardino, C., Bresciani, M., Stroppiana, D., Oggioni, A., Morabito, G., 2013. Optical remote sensing of lakes: an overview on Lake Maggiore. J. Limnol. 73.
Gons, H.J., Rijkeboer, M., Ruddick, K.G., 2002. A chlorophyll-retrieval algorithm for satellite imagery (Medium Resolution Imaging Spectrometer) of inland and coastal waters. J. Plankton Res. 24, 947–951.
Guo, L., Li, Z., 2003. Effects of nitrogen and phosphorus from fish cage-culture on the communities of a shallow lake in middle Yangtze River basin of China. Aquaculture 226, 201–212.
Hou, X., Feng, L., Duan, H., Chen, X., Sun, D., Shi, K., 2017. Fifteen-year monitoring of the turbidity dynamics in large lakes and reservoirs in the middle and lower basin of the Yangtze River, China. Remote Sens. Environ. 190, 107–121.
IOCCG, 2000. Remote Sensing of ocean colour in coastal, and other optically-complex, waters. In: Sathyendranath, S. (Ed.), Reports of the International Ocean-Colour Coordinating Group, No. 3, IOCCG, Dartmouth, Canada.

Jiang, H. (2010). Retrieval and Analysis Water Quality Parameters in Poyang Lake Based on Multi-source Remote Sensing Data. Nanchang: Nanchang University.
Jiang, G., Ma, R., Loiselle, S.A., Duan, H., Su, W., Cai, W., Huang, C., Yang, J., Yu, W., 2015. Remote sensing of particulate organic carbon dynamics in a eutrophic lake (Taihu Lake, China). Sci. Total Environ. 532, 245–254.
Jin, X., 1995. Lake environment in China. The Ocean Publishing Company, Beijing.
Knap, A.H., Michaels, A., Close, A.R., Ducklow, H., Dickson, A.G., 1994. (1994). Protocols for the Joint Global Ocean Flux Study (JGOFS) Core Measurements; IOC Manuals and Guides No. 29. United National Educational, Scientific and Cultural Organization (UNESCO), Paris, France.
Kong, F., Gao, G., 2005. Hypothesis on cyanobacteria bloom-forming mechanism in large shallow eutrophic lakes. Acta Ecol. Sin. 25, 589–595.
Kutser, T., Verpoorter, C., Paavel, B., Tranvik, L.J., 2015. Estimating lake carbon fractions from remote sensing data. Remote Sens. Environ. 157, 138–146.
Lee, Z., Carder, K.L., Mobley, C.D., Steward, R.G., Patch, J.S., 1998. Hyperspectral remote sensing for shallow waters. I. A semianalytical model. Appl. Opt. 37, 6329.
Lee, Z., Carder, K.L., Arnone, R.A., 2002. Deriving inherent optical properties from water color: a multiband quasi-analytical algorithm for optically deep waters. Appl. Opt. 41, 5755.
Liu, D., 2017. Estimation of Riverine Organic Carbon Flux Based on Remote Sensing and In-situ Data. Zhejiang University, Hangzhou.
Liu, D., Pan, D., Bai, Y., He, X., Wang, D., Zhang, L., 2015. Variation of dissolved organic carbon transported by two Chinese rivers: the Changjiang River and Yellow River. Mar. Pollut. Bull. 100, 60–69.
Lund, J.W., 1967. Eutrophication. Nature 214, 557–558.
Lyu, H., Wang, Q., Wu, C., Li, Z., Li, Y., Huang, J., 2015. Variations in optical scattering and backscattering by organic and inorganic particulates in Chinese lakes of Taihu, Chaohu and Dianchi. Chin. Geogr. Sci. 25, 26–38.
Ma, R., Tang, J., Dai, J., Zhang, Y., Song, Q., 2006. Absorption and scattering properties of water body in Taihu Lake, China: absorption. Int. J. Remote Sens. 27, 4277–4304.
Ma, R., Yang, G., Duan, H., Jiang, J., Wang, S., Feng, X., Li, A., Kong, F., Xue, B., Wu, J., Li, S., 2010. China's lakes at present: number, area and spatial distribution. Science China Earth Sciences 54, 283–289.
Markensten, H., Pierson, D.C., 2003. A dynamic model for flow and wind driven sediment resuspension in a shallow basin. Hydrobiologia 494, 305–311.
Meerhoff, M., Jeppesen, E., 2009. Shallow lakes and ponds. Encyclopedia of Inland Waters 645–655.
Mendonca, R., Muller, R.A., Clow, D., Verpoorter, C., Raymond, P., Tranvik, L.J., Sobek, S., 2017. Organic carbon burial in global lakes and reservoirs. Nat. Commun. 8, 1694.
Mueller, J.L., Fargion, G.S., McClain, C.R. (Eds.), 2003. Ocean Optics Protocols for Satellite Ocean Color Sensor Validation, Revision 4, Volume III: Radiometric Measurements and Data Analysis Protocols, NASA/TM-2003-211621/Rev4-Vol. III, NASA Goddard Space Flight Center, Greenbelt, Maryland (78 pp.).
Nelson, N.B., Prezelin, B.B., Bidigare, R.R., 1993. Phytoplankton light absorption and the package effect in California coastal waters. Mar. Ecol. Prog. Ser. 94, 217–227.
Oubelkheir, K., Claustre, H., Sciandra, A., Babin, M., 2005. Bio-optical and biogeochemical properties of different trophic regimes in oceanic waters. Limnology & Oceanography 50, 1795–1809.
Paerl, H.W., Xu, H., McCarthy, M.J., Zhu, G., Qin, B., Li, Y., Gardner, W.S., 2011. Controlling harmful cyanobacterial blooms in a hyper-eutrophic lake (Lake Taihu, China): the need for a dual nutrient (N & P) management strategy. Water Res. 45, 1973–1983.
Petus, C., Chust, G., Gohin, F., Doxaran, D., Froidefond, J.M., Sagarminaga, Y., 2010. Estimating turbidity and total suspended matter in the Adour River plume (South Bay of Biscay) using MODIS 250-m imagery. Cont. Shelf Res. 30, 379–392.
Preisendorfer, R.W., 1986. Secchi disk science: visual optics of natural waters. Limnology & Oceanography 31, 909–926.
Qin, B., 2004. Dynamics of sediment resuspension and the conceptual schema of nutrient release in the large shallow Lake Taihu, China. Chin. Sci. Bull. 49, 54.
Sharpley, A., Meyer, M., 1994. Minimizing agricultural nonpoint-source impacts: a symposium overview. J. Environ. Qual. 23, 1–3.
Shen, M., Duan, H., Cao, Z., Xue, K., Loiselle, S., Yesou, H., 2017. Determination of the downwelling diffuse attenuation coefficient of lake water with the Sentinel-3A OLCI. Remote Sens. 9, 1246.
Shi, K., Li, Y., Li, L., Lu, H., 2013. Absorption characteristics of optically complex inland waters: implications for water optical classification. Journal of Geophysical Research: Biogeosciences 118, 860–874.
Shi, K., Zhang, Y., Xu, H., Zhu, G., Qin, B., Huang, C., Liu, X., Zhou, Y., Lv, H., 2015a. Long-term satellite observations of microcystin concentrations in Lake Taihu during cyanobacterial bloom periods. Environmental Science & Technology 49, 6448–6456.
Shi, K., Zhang, Y., Zhu, G., Liu, X., Zhou, Y., Xu, H., Qin, B., Liu, G., Li, Y., 2015b. Long-term remote monitoring of total suspended matter concentration in Lake Taihu using 250m MODIS-Aqua data. Remote Sens. Environ. 164, 43–56.
Simis, S.G.H., Peters, S.W.M., Gons, H.J., 2005. Remote sensing of the cyanobacterial pigment phycocyanin in turbid inland water. Limnology & Oceanography 50, 237–245.
Spinrad, R.W., Mitchell, B.G., 1990. Algorithms for Determining the Absorption Coefficient for Aquatic Particulates Using the Quantitative Filter Technique. 1302 p. 137.
Strickland, J.D.H., Parsons, T.R., 1972. A practical handbook of seawater analysis. Bulletin 167.
Tao, S., Fang, J., Zhao, X., Zhao, S., Shen, H., Hu, H., Tang, Z., Wang, Z., Guo, Q., 2015. Rapid loss of lakes on the Mongolian Plateau. Proc. Natl. Acad. Sci. U. S. A. 112, 2281–2286.
Toming, k., Kutser, T., Uiboupin, R., Arikas, A., Vahter, K., Paavel, B., 2017. Mapping water quality parameters with Sentinel-3 ocean and land colour instrument imagery in the Baltic Sea. Remote Sens. 9, 1070.
Tong, Y., Zhang, W., Wang, X., Couture, R.M., Larssen, T., Zhao, Y., Li, J., Liang, H., Liu, X., Bu, X., 2017. Decline in Chinese lake phosphorus concentration accompanied by shift in sources since 2006. Nat. Geosci. 10, 12–2017.
Wang, J., Wang, J., 1984. Some problems in the conversion among chlorophyll a, biomass, and production of phytoplankton. Wuhan Botanical Research 2, 249–258.
Wang, M., Liu, X., Zhang, J., 2002. Evaluate method and classification standard on lake eutrophication (in Chinese). Environmental Monitoring in China 18, 47–49.
Wang, W.-q., Dong, Q., Shang, S.-l., Wu, J.-y., Lee, Z.-p, 2009. An evaluation of two semi-analytical ocean color algorithms for waters of the South China Sea. Journal of Tropical Oceanography 28, 35–42.
Wang, X., Ma, H., Li, R., Song, Z., Wu, J., 2012. Seasonal fluxes and source variation of organic carbon transported by two major Chinese Rivers: the Yellow River and Changjiang (Yangtze) River. Glob. Biogeochem. Cycles 26.
Wang, J., Sheng, Y., Tong, T.S.D., 2014. Monitoring decadal lake dynamics across the Yangtze Basin downstream of Three Gorges Dam. Remote Sens. Environ. 152, 251–269.
Wang, S., Li, J., Zhang, B., Spyrakos, E., Tyler, A.N., Shen, Q., Zhang, F., Kutser, T., Lehmann, M.K., Wu, Y., Peng, D., 2018. Trophic state assessment of global inland waters using a MODIS-derived Forel-Ule index. Remote Sens. Environ. 217, 444–460.
Wu, J.-H., Duan, H.-T., Zhang, Y.-C., Ma, R.-H., 2015. A novel algorithm to estimate POC concentration in Chaohu Lake, China. Journal of Infrared and Millimeter Waves 34, 725–731.
Xu, H., Paerl, H.W., Qin, B.Q., Zhu, G.W., Gao, G.A., 2010. Nitrogen and phosphorus inputs control phytoplankton growth in eutrophic Lake Taihu, China. Limnology & Oceanography 55, 420–432.
Xue, K., Zhang, Y., Duan, H., Ma, R., Loiselle, S., Zhang, M., 2015. A Remote Sensing approach to estimate vertical profile classes of phytoplankton in a eutrophic lake. Remote Sens. 7, 14403–14427.
Xue, K., Zhang, Y., Duan, H., Ma, R., 2017. Variability of light absorption properties in optically complex inland waters of Lake Chaohu, China. J. Great Lakes Res. 43, 17–31.
Ylöstalo, P., Kallio, K., Seppälä, J., 2014. Absorption properties of in-water constituents and their variation among various lake types in the boreal region. Remote Sens. Environ. 148, 190–205.
Zhang, Y., Qin, B., Zhu, G., Gao, G., Luo, L., Chen, W., 2006. Effect of sediment resuspension on underwater light field in shallow lakes in the middle and lower reaches of the Yangtze River: a case study in Longgan Lake and Taihu Lake. Science in China: Series D Earth Sciences 49, 114–125.
Zhang, Y., Zhang, E., Yin, Y., van Dijk, M.A., Feng, L., Shi, Z., Liu, M., Qina, B., 2010. Characteristics and sources of chromophoric dissolved organic matter in lakes of the Yungui Plateau, China, differing in trophic state and altitude. Limnology & Oceanography 55, 2645–2659.
Zhang, L., Xue, M., Wang, M., Cai, W.-J., Wang, L., Yu, Z., 2014. The spatiotemporal distribution of dissolved inorganic and organic carbon in the main stem of the Changjiang (Yangtze) River and the effect of the Three Gorges Reservoir. Journal of Geophysical Research: Biogeosciences 119, 741–757.
Zhang, Y., Shi, K., Zhou, Y., Liu, X., Qin, B., 2016. Monitoring the river plume induced by heavy rainfall events in large, shallow, Lake Taihu using MODIS 250m imagery. Remote Sens. Environ. 173, 109–121.
Zhang, G., Yao, T., Chen, W., Zheng, G., Shum, C.K., Yang, K., Piao, S., Sheng, Y., Yi, S., Li, J., O'Reilly, C.M., Qi, S., Shen, S.S.P., Zhang, H., Jia, Y., 2019. Regional differences of lake evolution across China during 1960s–2015 and its natural and anthropogenic causes. Remote Sens. Environ. 221, 386–404.